Zeeman Effect in Centrosymmetric Antiferromagnetic Semiconductors Controlled by an Electric Field

Hong Jian Zhao,[1,2,3] Xinran Liu,[1] Yanchao Wang,[1,4,*] Yurong Yang,[5] Laurent Bellaiche,[6] and Yanming Ma[1,3,4,†]

[1]*International Center for Computational Method and Software, College of Physics, Jilin University, Changchun 130012, China*
[2]*Key Laboratory of Physics and Technology for Advanced Batteries (Ministry of Education), College of Physics, Jilin University, Changchun 130012, China*
[3]*International Center of Future Science, Jilin University, Changchun 130012, China*
[4]*State Key Laboratory of Superhard Materials, College of Physics, Jilin University, Changchun 130012, China*
[5]*National Laboratory of Solid State Microstructures and Jiangsu Key Laboratory of Artificial Functional Materials, Department of Materials Science and Engineering, Nanjing University, Nanjing 210093, China*
[6]*Physics Department and Institute for Nanoscience and Engineering, University of Arkansas, Fayetteville, Arkansas 72701, USA*

(Received 2 May 2022; accepted 16 September 2022; published 24 October 2022)

Centrosymmetric antiferromagnetic semiconductors, although abundant in nature, seem less promising than ferromagnets and ferroelectrics for practical applications in semiconductor spintronics. As a matter of fact, the lack of spontaneous polarization and magnetization hinders the efficient utilization of electronic spin in these materials. Here, we propose a paradigm to harness electronic spin in centrosymmetric antiferromagnets via Zeeman spin splitting of electronic energy levels—termed as the spin Zeeman effect—which is controlled by an electric field. By symmetry analysis, we identify 21 centrosymmetric magnetic point groups that accommodate such a spin Zeeman effect. We further predict by first principles that two antiferromagnetic semiconductors, Fe_2TeO_6 and $SrFe_2S_2O$, are excellent candidates showcasing Zeeman splittings as large as ∼55 and ∼30 meV, respectively, induced by an electric field of 6 MV/cm. Moreover, the electronic spin magnetization associated to the splitting energy levels can be switched by reversing the electric field. Our Letter thus sheds light on the electric-field control of electronic spin in antiferromagnets, which broadens the scope of application of centrosymmetric antiferromagnetic semiconductors.

DOI: 10.1103/PhysRevLett.129.187602

Introduction.—In semiconductors, the creation of magnetically or electrically controllable spin splittings with relatively large magnitudes is at the heart of designing semiconductor spintronic devices (e.g., spin transistor) [1–5]. The conventional ferroelectric or ferromagnetic semiconductors naturally host such controllable spin splittings because of the existence of a spontaneous polarization or magnetization, thanks to the Rashba-Dresselhaus [4–7], or Zeeman [1,8] effect. In sharp contrast, the centrosymmetric antiferromagnetic semiconductors do not have any polarization, and their magnetization is either null or tiny. The lack of polarization and magnetization makes it challenging to generate a sizable and controllable spin splitting, by magnetic or electric field, in centrosymmetric antiferromagnetic semiconductors. Consequently, the centrosymmetric antiferromagnetic semiconductors—in spite of their abundance in nature—seem not promising for practical applications in spintronics [9–14].

Recently, efforts were made to explore the possible spin splittings hosted by *all* types of magnetic space groups, involving nonmagnetic, ferromagnetic, and antiferromagnetic materials (see, e.g., Refs. [14–21]). Several previously overlooked spin-splitting patterns were discovered [14–21], but without explicitly demonstrating the possibility of creating and controlling sizable spin splittings in centrosymmetric antiferromagnets by magnetic or electric field. Interestingly, two works focusing on the nonlinear photocurrent in $MnBi_2Te_4$ [22] and magneto-optic Kerr effect in $MnPSe_3$ [23] (rather than spin splittings) hint to such a possibility. However, the general conditions and underlying mechanisms to the creation and control of spin splittings by magnetic or electric field in centrosymmetric antiferromagnets remain elusive.

In this Letter, we aim at exploring spin splittings that would be controllable by electric field and hosted by centrosymmetric antiferromagnets. Our basic idea is rooted in the magnetoelectric effect (see, e.g., Ref. [24]). As a matter of fact, an electric field not only creates polarization P_α but also generates magnetization $M_\beta \propto P_\alpha$ in magnetoelectric antiferromagnets ($\alpha, \beta = x, y, z$) [24]. The occurrence of M_β implies an effective internal magnetic field $B_\beta^{\text{eff}} \propto P_\alpha$ in materials, which couples with electronic spin σ_β (i.e., Pauli matrix σ_β) and yields a Zeeman-like Hamiltonian $\lambda_{\alpha,\beta} P_\alpha \sigma_\beta$ [25].

Further, we check our idea by symmetry analysis and first-principles simulations. We identify 21 centrosymmetric magnetic point groups (MPGs) that accommodate electrically controllable Zeeman spin splittings. More promisingly,

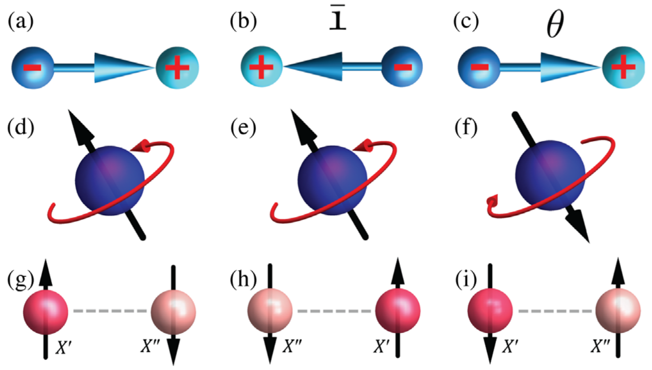

FIG. 1. The transformations of polarization P_α [panels (a)–(c)], spin angular momentum S_β [panels (d)–(f)], and magnetic structure X [panels (g)–(i)], under inversion $\bar{1}$ and time reversal θ. In (a)–(c), the "+" and "−" signs denote the positive and negative charges, respectively. In (d)–(f), the black arrow sketches the direction of S_β, while the red curly arrow "depicts" spin. In (g)–(i), the black arrow represents the magnetic moment carried by X' or X'' ions. The inversion center locates in the middle of the "+" and "−" spheres [panels (a)–(c)], at the center of the purple ball [panels (d)–(f)], or at the midpoint of X' and X'' spheres [panels (g)–(i)], respectively.

we find two centrosymmetric antiferromagnetic semiconductors, Fe_2TeO_6 and $SrFe_2S_2O$, in which large Zeeman spin splittings of ~55 and ~30 meV can be created by an electric field of 6 MV/cm, respectively. The electronic spin magnetization associated to the splitting energy levels is confirmed to be switchable by reversing the electric field.

Couplings between polarization and spin.—Among 122 MPGs, there are 11 groups, namely, $\bar{1}1'$, $2/m1'$, $mmm1'$, $4/m1'$, $4/mmm1'$, $\bar{3}1'$, $\bar{3}m1'$, $6/m1'$, $6/mmm1'$, $m\bar{3}1'$, and $m\bar{3}m1'$, that contain both inversion $\bar{1}$ and time-reversal θ symmetries [26,27]. As will be shown below, these 11 groups—belonging to type-II Shubnikov MPGs (denoted by G')—host a sequence of subgroups (i.e., type-III Shubnikov MPGs) that allow the couplings between polarization and spin. Here, G' can be uniformly written as $G' = G \cup \theta G$, where $G = G_0 \cup \bar{1}G_0$ is the crystallographic point group and G_0 is the subgroup of G containing *only* proper rotations [27–29]. We aim to find the minimal couplings involving electric polarization and spin with respect to the G' group. To this end, we examine the transformation behaviors of electric polarization P_α and spin angular momentum operator S_β under $\bar{1}$ and θ, where $\alpha, \beta = x, y, z$ denote the Cartesian components (see Fig. 1). Normally, the coupling $P_\alpha S_\beta$ (if existing) implies the electronic spin splittings induced by polarization P_α, recalling that spin splitting is characterized by σ_β where $S_\beta = (\hbar/2)\sigma_\beta$. Figures 1(a)–1(f) indicate the following transformation rules, namely, $\bar{1}$: $P_\alpha \to -P_\alpha$, $S_\beta \to S_\beta$, $\sigma_\beta \to \sigma_\beta$ and θ: $P_\alpha \to P_\alpha$, $S_\beta \to -S_\beta$, $\sigma_\beta \to -\sigma_\beta$. Hence, the bilinear coupling between polarization and spin does not exist in the presence of either inversion or time-reversal symmetry, because $\bar{1}$: $P_\alpha\sigma_\beta \to -P_\alpha\sigma_\beta$; θ: $P_\alpha\sigma_\beta \to -P_\alpha\sigma_\beta$.

We move on to explore whether the trilinear coupling $XP_\alpha\sigma_\beta$ does exist or not with respect to G'. First, to fulfill the inversion and time-reversal symmetries, X should be a quantity such that $\bar{1}$: $X \to -X$ and θ: $X \to -X$. Figures 1(g)–1(i) showcase such a possible X extracted from an antiferromagnetic structure. For demonstrating purposes, we simply assume that the X quantity, namely, magnetic order parameter, is formed by two atoms labeled X' and X'', where X' and X'' are of the same atomic species, but carry magnetic moments along opposite directions [see Fig. 1(g)]. Under inversion $\bar{1}$, X' and X'' atoms swap their positions, while their carried magnetic moments remain unchanged [see Fig. 1(h)]; Under time reversal θ, X' and X'' atoms remain in place with the magnetic moments being flipped [see Fig. 1(i)]. This leads to $\bar{1}$: $X \to -X$ and θ: $X \to -X$. Therefore, $XP_\alpha\sigma_\beta$ is compatible with inversion and time-reversal symmetries. Next, $XP_\alpha\sigma_\beta$ should be allowed by the proper rotation operations in G_0. The $\bar{1}1'$ is the simplest case to tackle, because its corresponding G_0 group only contains identity symmetry. Consequently, nine different couplings $XP_\alpha\sigma_\beta$ with $\alpha, \beta = x, y, z$ are permitted by symmetry operations of the $\bar{1}1'$ group. Unfortunately, the situation for the remaining ten type-II Shubnikov MPGs is quite complicated, since the G_0 group contains more symmetry operations than identity, leading to an additional symmetry constraint for $XP_\alpha\sigma_\beta$. For instance, 2_z, rotation of π along the z direction, transforms P_x, P_z, and σ_z as 2_z: $P_z \to P_z$, $P_x \to -P_x$, $\sigma_z \to \sigma_z$. As a result, 2_z transforms $XP_z\sigma_z$ and $XP_x\sigma_z$ via 2_z: $XP_z\sigma_z \to XP_z\sigma_z$, $XP_x\sigma_z \to -XP_x\sigma_z$, assuming that X is invariant under 2_z. In this case, $XP_z\sigma_z$ is allowed by 2_z rotation, while $XP_x\sigma_z$ is not. Using this logic, we have conducted symmetry analysis regarding these 10 type-II Shubnikov MPGs, shown in Sec. I of the Supplemental Material [30] (containing Refs. [31–55]). Taking $mmm1'$ as an example [see Eq. (S7) and Sec. I.3 of the Supplemental Material [30]], the symmetry-allowed trilinear couplings associated with $X \equiv M(A_u)$ are given by $\lambda'_{x,x}M(A_u)P_x\sigma_x + \lambda'_{y,y}M(A_u)P_y\sigma_y + \lambda'_{z,z}M(A_u)P_z\sigma_z$, where $\lambda'_{x,x}$, $\lambda'_{y,y}$, and $\lambda'_{z,z}$ are coefficients characterizing the coupling strength. To understand the physical meaning of $XP_\alpha\sigma_\beta$ coupling, let us recall that $XP_\alpha\sigma_\beta$ is reminiscent of the conventional Zeeman term $B_\beta\sigma_\beta$ [1,56]. This indicates that polarization P_α can generate in materials—via a secondary effect—an effective magnetic field $B_\beta^{\mathrm{eff}} \propto XP_\alpha$, whose microscopic origin may be roughly thought of as follows: a polar distortion modifies electronic wave functions and ligand field in materials, yielding an internal effective magnetic field [24]. Such an effective field B_β^{eff} causes Zeeman spin splitting.

Now we demonstrate how to search for real materials hosting $XP_\alpha\sigma_\beta$ coupling. First of all, note that the existence of order parameter X breaks inversion $\bar{1}$, time reversal θ, and/or some other symmetry operations of the G' group. Such symmetry breaking lowers the symmetry of the system from the G' group to its subgroup g' which contains the operations that are not broken by X. In such sense, X is invariant under *all* the symmetry operations of g'. With respect to the g' group, the effective Hamiltonian term $\lambda'_{\alpha,\beta}XP_\alpha\sigma_\beta$ can be rewritten as $\lambda_{\alpha,\beta}P_\alpha\sigma_\beta$, noting that the quantity X is absorbed by the coefficient $\lambda'_{\alpha,\beta}$. Therefore, to find a real material hosting X order parameter and $\lambda_{\alpha,\beta}P_\alpha\sigma_\beta$ coupling, effort should be made to search for materials with magnetic point group g'. Following this logic, we conduct symmetry analysis for the 11 aforementioned type-II Shubnikov MPGs, in order to extract the possible g' groups from G' (see Sec. I of the Supplemental Material [30] for the derivations). In particular, we find 21 type-III Shubnikov MPGs that accommodate the $\lambda_{\alpha,\beta}P_\alpha\sigma_\beta$ couplings, as summarized in Table I (see Sec. I.12 and Table S13 of the Supplemental Material [30] for more details). Interestingly, our derived Zeeman coupling coefficients (Table I) are similar to the tabulated magnetoelectric tensors [57]. In such sense, our proposed 21 MPGs also host the magnetoelectric effect, in agreement with our aforementioned analysis (see *Introduction*). These MPGs do not have inversion $\bar{1}$ or time reversal θ, but rather exhibit parity-time symmetry ($\bar{1}\theta$). In essence, these 21 type-III Shubnikov MPGs are centrosymmetric in the four-dimensional spacetime, since the $\bar{1}\theta$ symmetry operation transforms the spatial-temporal coordinate (x, y, z, t) to $(-x, -y, -z, -t)$. Hence, none of these 21 MPGs hosts spontaneous ferromagnetism or electric polarization. According to the $\lambda_{\alpha,\beta}P_\alpha\sigma_\beta$ coupling, the $\bar{1}\theta$ symmetry operation is broken in the presence of polarization, yielding Zeeman-type spin splittings. This coincides with the previous symmetry analysis which indicates that the breakdown of parity-time symmetry can generate spin splittings (see, e.g., Refs. [14–16,22,23,58–60]).

Taking $m'm'm'$ as an example, Table I indicates the $\lambda_{x,x}$, $\lambda_{y,y}$, and $\lambda_{z,z}$ couplings, yielding the effective Hamiltonian $H(m'm'm') = \lambda_{x,x}P_x\sigma_x + \lambda_{y,y}P_y\sigma_y + \lambda_{z,z}P_z\sigma_z = \kappa_{x,x}\mathcal{E}_x\sigma_x + \kappa_{y,y}\mathcal{E}_y\sigma_y + \kappa_{z,z}\mathcal{E}_z\sigma_z$, where $\mathcal{E}_\alpha$ is the electric field along the α direction [61]. Similarly, the effective Hamiltonians for $4/m'm'm'$ and $\bar{3}'m'$ are given by $H(4/m'm'm') = \kappa_{x,x}(\mathcal{E}_x\sigma_x + \mathcal{E}_y\sigma_y) + \kappa_{z,z}\mathcal{E}_z\sigma_z$ and $H(\bar{3}'m') = \kappa_{x,x}(\mathcal{E}_x\sigma_x + \mathcal{E}_y\sigma_y) + \kappa_{z,z}\mathcal{E}_z\sigma_z$, respectively. Note that the splittings predicted by $H(\bar{3}'m')$ were claimed to be critical for the nonlinear photocurrent effect in topological material $MnBi_2Te_4$ [22].

Creating and controlling Zeeman splittings in $SrFe_2S_2O$ *and* Fe_2TeO_6.—Based on Table I, we search from the MAGNDATA database [51] for antiferromagnets with Zeeman splittings that can be created and controlled by an electric field. Promisingly, we find two antiferromagnetic semiconductors, $SrFe_2S_2O$ and Fe_2TeO_6 (see Fig. 2), whose Néel temperatures are both higher than 200 K [62–64]. The corresponding MPGs for $SrFe_2S_2O$ and Fe_2TeO_6 are $m'm'm'$ [62] and $4/m'm'm'$ [64], respectively. Employing their ground state magnetic structures [sketched in Figs. 2(b) and 2(d)] and considering spin-orbit interaction, we use first principles to compute the band structures of $SrFe_2S_2O$ and Fe_2TeO_6 without polarization or with polarization created by an electric field of 6 MV/cm (see Sec. III.1 of the Supplemental Material [30]). As shown in Fig. S2 of the Supplemental Material [30], the valence band maximum (VBM) of $SrFe_2S_2O$ is located at the Γ point, and the corresponding spin levels are (i) degenerate for nonpolarized, (ii) nearly degenerate for $\mathcal{E}_x$ polarized, (iii) slightly split for $\mathcal{E}_z$ polarized, and (iv) obviously split for $\mathcal{E}_y$ polarized $SrFe_2S_2O$ material. As for Fe_2TeO_6, the conduction band minimum (CBM) is at the Γ point, and $\mathcal{E}_z$ apparently splits the spin levels at the CBM (see Fig. S5 of the Supplemental Material [30]) [65]. Our numerical simulations further indicate that the magnitudes of Zeeman spin splittings are in perfect linear relationship with $\mathcal{E}_\alpha$ (see Fig. 3). Strikingly, $\mathcal{E}_y = 6$ MV/cm and $\mathcal{E}_z = 6$ MV/cm generate Zeeman spin splittings of ~30 meV and ~55 meV [66], respectively, for the VBM of $SrFe_2S_2O$ and CBM of Fe_2TeO_6.

TABLE I. The couplings that are hosted by 21 type-III Shubnikov MPGs. In each (P_α, σ_β) entry, $\lambda_{\alpha,\beta}$ indicates the coupling $\lambda_{\alpha,\beta}P_\alpha\sigma_\beta$; the "…" implies that the coupling $P_\alpha\sigma_\beta$ is forbidden by symmetry. To better understand this table, we refer the readers to Sec. I.12 of the Supplemental Material [30].

	P_x			P_y			P_z		
	σ_x	σ_y	σ_z	σ_x	σ_y	σ_z	σ_x	σ_y	σ_z
$\bar{1}'$	$\lambda_{x,x}$	$\lambda_{x,y}$	$\lambda_{x,z}$	$\lambda_{y,x}$	$\lambda_{y,y}$	$\lambda_{y,z}$	$\lambda_{z,x}$	$\lambda_{z,y}$	$\lambda_{z,z}$
$2/m'$	$\lambda_{x,x}$	$\lambda_{x,y}$	…	$\lambda_{y,x}$	$\lambda_{y,y}$	…	…	…	$\lambda_{z,z}$
$2'/m$	…	…	$\lambda_{x,z}$	…	…	$\lambda_{y,z}$	$\lambda_{z,x}$	$\lambda_{z,y}$	…
$m'm'm'$	$\lambda_{x,x}$	…	…	…	$\lambda_{y,y}$	…	…	…	$\lambda_{z,z}$
mmm'	…	$\lambda_{x,y}$	…	$\lambda_{y,x}$	…	…	…	…	…
$mm'm$	…	…	$\lambda_{x,z}$	…	…	…	$\lambda_{z,x}$	…	…
$m'mm$	…	…	…	…	…	$\lambda_{y,z}$	…	$\lambda_{z,y}$	…
$4/m'$	$\lambda_{x,x}$	$\lambda_{x,y}$	…	$-\lambda_{x,y}$	$\lambda_{x,x}$	…	…	…	$\lambda_{z,z}$
$4'/m'$	$\lambda_{x,x}$	$\lambda_{x,y}$	…	$\lambda_{x,y}$	$-\lambda_{x,x}$	…	…	…	…
$4/m'm'm'$	$\lambda_{x,x}$	…	…	…	$\lambda_{x,x}$	…	…	…	$\lambda_{z,z}$
$4/m'mm$	…	$\lambda_{x,y}$	…	$-\lambda_{x,y}$	…	…	…	…	…
$4'/m'm'm$	$\lambda_{x,x}$	…	…	…	$-\lambda_{x,x}$	…	…	…	…
$4'/m'mm'$	…	$\lambda_{x,y}$	…	$\lambda_{x,y}$	…	…	…	…	…
$\bar{3}'$	$\lambda_{x,x}$	$\lambda_{x,y}$	…	$-\lambda_{x,y}$	$\lambda_{x,x}$	…	…	…	$\lambda_{z,z}$
$\bar{3}'m'$	$\lambda_{x,x}$	…	…	…	$\lambda_{x,x}$	…	…	…	$\lambda_{z,z}$
$\bar{3}'m$	…	$\lambda_{x,y}$	…	$-\lambda_{x,y}$	…	…	…	…	…
$6/m'$	$\lambda_{x,x}$	$\lambda_{x,y}$	…	$-\lambda_{x,y}$	$\lambda_{x,x}$	…	…	…	$\lambda_{z,z}$
$6/m'm'm'$	$\lambda_{x,x}$	…	…	…	$\lambda_{x,x}$	…	…	…	$\lambda_{z,z}$
$6/m'mm$	…	$\lambda_{x,y}$	…	$-\lambda_{x,y}$	…	…	…	…	…
$m'\bar{3}'$	$\lambda_{x,x}$	…	…	…	$\lambda_{x,x}$	…	…	…	$\lambda_{x,x}$
$m'\bar{3}'m'$	$\lambda_{x,x}$	…	…	…	$\lambda_{x,x}$	…	…	…	$\lambda_{x,x}$

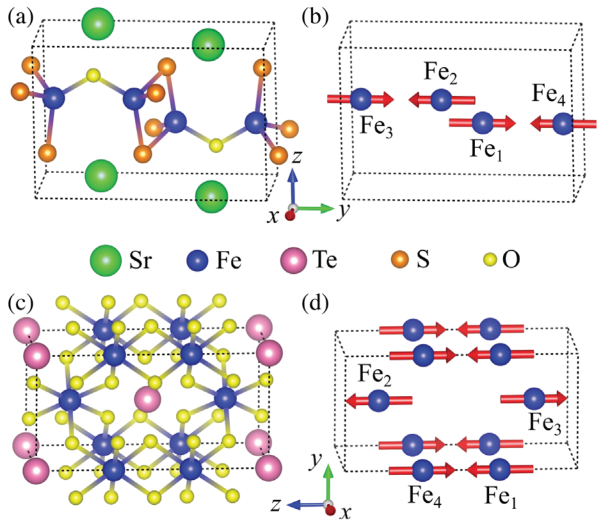

FIG. 2. Panels (a) and (c) show the crystal structures of $SrFe_2S_2O$ and Fe_2TeO_6, respectively. Panels (b) and (d) sketch the ground state magnetic structures of $SrFe_2S_2O$ (magnetic space group: $Pm'm'n'$ [62]) and Fe_2TeO_6 (magnetic space group: $P4_2/m'n'm'$ [64]), respectively.

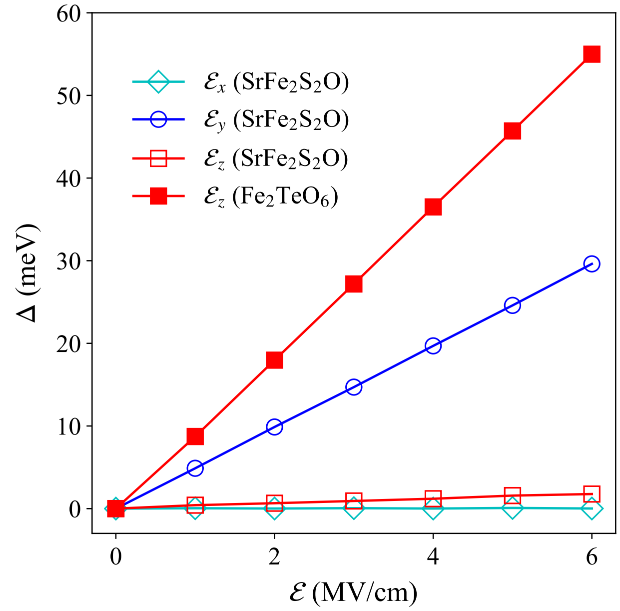

FIG. 3. The Zeeman spin splittings for the VBM of $SrFe_2S_2O$ and the CBM of Fe_2TeO_6, as a function of electric field $\mathcal{E}$. We first determine the crystal structures (i.e., ionic degrees of freedom) of $SrFe_2S_2O$ and Fe_2TeO_6 under each electric field, via a first-principles-based approach (see, e.g., Ref. [67]). For each determined crystal structure, we then compute the energy levels and extract the Zeeman spin splitting at the Γ point. Note that during the calculation for energy levels, no electric field is considered any more.

On the other hand, we notice that the spin splittings induced by $\mathcal{E}_x$, $\mathcal{E}_y$, and $\mathcal{E}_z$ in $SrFe_2S_2O$ exhibit highly distinct characteristics (see Fig. 3). For example, the electric field $\mathcal{E}_x$ of 6 MV/cm causes nearly null Zeeman spin splitting, implying the smallness of the coupling coefficient $\kappa_{x,x}$ in $H(m'm'm') = \kappa_{x,x}\mathcal{E}_x\sigma_x + \kappa_{y,y}\mathcal{E}_y\sigma_y + \kappa_{z,z}\mathcal{E}_z\sigma_z$. Meanwhile, the Zeeman spin splitting induced by $\mathcal{E}_y$ is far larger than that generated by $\mathcal{E}_z$ of the same magnitude as $\mathcal{E}_y$. For interpretation, we analyze the spin magnetization (S_x, S_y, S_z) associated with the two top most energy sublevels at the Γ point. When polarizing $SrFe_2S_2O$ by the $\mathcal{E}_\alpha$ ($\alpha = x, y, z$) electric field, an effective magnetic field $B_\alpha^{\mathrm{eff}} \propto \mathcal{E}_\alpha$ is created in the material. The B_α^{eff} field couples with S_α, causing a Zeeman energy proportional to $\pm B_\alpha^{\mathrm{eff}} S_\alpha$, where the $\pm$ sign characterizes the sublevels whose α spin magnetization component are positive or negative. Polarizing $SrFe_2S_2O$ by $\mathcal{E}_y = 6$ MV/cm and $\mathcal{E}_z = 6$ MV/cm leads to the spin magnetization of $S_y \approx \pm 0.74$ and $S_z \approx \pm 0.08$, respectively. The predominant S_y component implies that the Zeeman spin splitting created by $\mathcal{E}_y$ is the most prominent. Our further analysis regarding the orbital-projected spin magnetization for $SrFe_2S_2O$ can be found in Sec. III.2 of the Supplemental Material [30].

We now address whether the spin magnetization S_α for $SrFe_2S_2O$ and Fe_2TeO_6 are switchable by electric field. To begin with, let us recall our model $H(m'm'm') = \kappa_{x,x}\mathcal{E}_x\sigma_x + \kappa_{y,y}\mathcal{E}_y\sigma_y + \kappa_{z,z}\mathcal{E}_z\sigma_z$ for $SrFe_2S_2O$ ($m'm'm'$ group). In the presence of $\mathcal{E}_y$, the spin levels will be split into two sublevels $E_+ = \kappa_{y,y}\mathcal{E}_y$ (eigenstate being $|+\rangle$) and $E_- = -\kappa_{y,y}\mathcal{E}_y$ (eigenstate being $|-\rangle$), where $\sigma_y|+\rangle = |+\rangle$ and $\sigma_y|-\rangle = -|-\rangle$. The spin magnetization S_y associated with $\kappa_{y,y}\mathcal{E}_y$ and $-\kappa_{y,y}\mathcal{E}_y$ are thus $\frac{1}{2}\langle+|\sigma_y|+\rangle = \frac{1}{2}$ and $\frac{1}{2}\langle-|\sigma_y|-\rangle = -\frac{1}{2}$ [68]. When reversing the electric field from $\mathcal{E}_y$ to $-\mathcal{E}_y$, the two split sublevels become $E_- = \kappa_{y,y}\mathcal{E}_y$ and $E_+ = -\kappa_{y,y}\mathcal{E}_y$, with the corresponding eigenstates given by $|-\rangle$ and $|+\rangle$; Consequently, the $\kappa_{y,y}\mathcal{E}_y$ and $-\kappa_{y,y}\mathcal{E}_y$ sublevels are linked with the spin magnetization S_y of $-\frac{1}{2}$ and $\frac{1}{2}$, respectively. Similarly, our models $H(m'm'm')$ and $H(4/m'm'm') = \kappa_{x,x}(\mathcal{E}_x\sigma_x + \mathcal{E}_y\sigma_y) + \kappa_{z,z}\mathcal{E}_z\sigma_z$ predict that reversing electric field $\mathcal{E}_\alpha$ will switch the S_α spin magnetization between $\pm\frac{1}{2}$ and $\mp\frac{1}{2}$. To confirm our predictions, we compute the local band structures, along with spin magnetization S_y or S_z, for $SrFe_2S_2O$ and Fe_2TeO_6 (see Fig. 4), including the spin-orbit interaction [69]. We focus on the local bands around the VBM of $SrFe_2S_2O$ and the CBM of Fe_2TeO_6. When reversing the electric field from $\mathcal{E}_y = +6$ MV/cm to $\mathcal{E}_y = -6$ MV/cm (respectively, from $\mathcal{E}_z = +6$ MV/cm to $\mathcal{E}_z = -6$ MV/cm), the S_y for $SrFe_2S_2O$ (respectively, S_z for Fe_2TeO_6) is switchable. We further find that the S_z component of $SrFe_2S_2O$ can also be switched by $\mathcal{E}_z$, although the S_z at the VBM is quite small (see Fig. S4 of the Supplemental Material [30]) [70]. Those results are in qualitative agreement with our model analysis.

To complete this section, let us comment on the limitation of our models. As mentioned above, our models

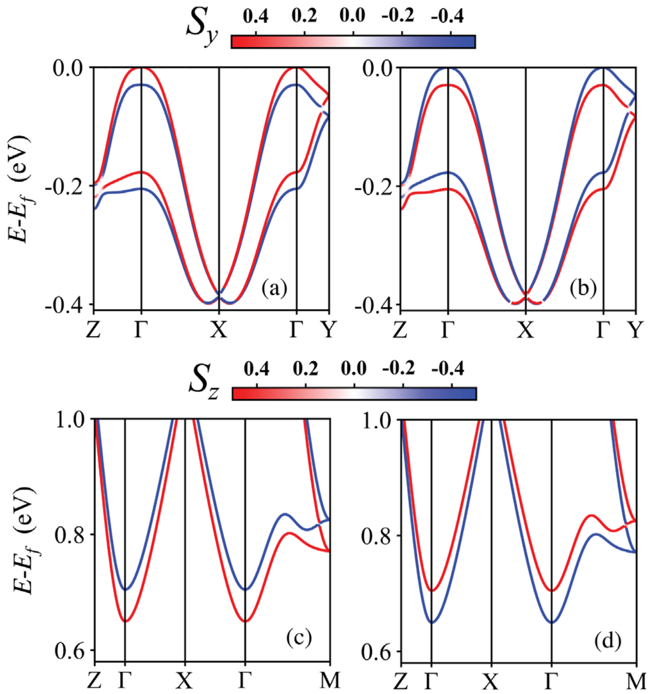

FIG. 4. Panels (a) and (b) are local band structures of $SrFe_2S_2O$ polarized by $\mathcal{E}_y = +6$ MV/cm and $\mathcal{E}_y = -6$ MV/cm, respectively. Panels (c) and (d) show local band structures of Fe_2TeO_6 polarized by $\mathcal{E}_z = +6$ MV/cm and $\mathcal{E}_z = -6$ MV/cm, respectively. The color bar corresponds to S_y or S_z. The Fermi level E_f is set as the VBM.

predict S_α as $\pm\frac{1}{2}$ for $SrFe_2S_2O$, under electric field $\mathcal{E}_\alpha$. This is at odds with our first-principles simulations, which give, e.g., $S_y \approx \pm 0.74$ and $S_z \approx \pm 0.08$ for $SrFe_2S_2O$ polarized by $\mathcal{E}_y = 6$ MV/cm and $\mathcal{E}_z = 6$ MV/cm, respectively. Note that the value $S_z = \pm\frac{1}{2}$ (predicted by our model) can be ~6 times larger than the first-principles-predicted magnitudes (i.e., $S_z \approx \pm 0.08$ of $\mathcal{E}_z$-polarized $SrFe_2S_2O$). Such an inconsistency arises from the fact that that our models incorporate *only* the minimal couplings involving electronic spin, electric field, and a mediated magnetic structure. Other degrees of freedom such as atomic orbitals and electronic wave vectors are neglected. More explicitly, our models consider merely two spin sublevels, while the first-principles calculations consider various degrees of freedom (e.g., the 3*d* orbitals of Fe ions), forming a multiband case. As such, our models could only reveal the electric field induced Zeeman splittings qualitatively (i.e., not quantitatively).

Summary and outlook.—We have shown that the electric field can create Zeeman spin splittings in centrosymmetric antiferromagnetic semiconductors belonging to one of the 21 MPGs (Table I). By first-principles simulations, we further identify two real materials, Fe_2TeO_6 and $SrFe_2S_2O$, that accommodate Zeeman spin splittings as large as ~55 and ~30 meV, respectively, in the presence of an electric field of 6 MV/cm. The resulting Zeeman spin splittings are controllable by an electric field, and can possibly be detected by some approaches (e.g., optical and transport measurements) that are well-established in spintronics [1,2,71]. This will open a door toward the utilization of electronic spin in centrosymmetric antiferromagnetic semiconductors, emphasizing the importance of such materials for fabricating semiconductor spintronic devices. To finish, we hope that our discoveries will not only deepen the knowledge of magnetoelectric interactions, but also motivate a sequence of innovative studies in the emerging research directions of antiferromagnetic spintronics [9–13,72,73] and semiconductor spintronics [1,2,8,56,71].

This research was supported by the National Natural Science Foundation of China under Grants No. T2225013, No. 12274174, No. 12174142, No. 12034009, No. 11874207, the Program for JLU Science and Technology Innovative Research Team, and the Science Challenge Project No. TZ2016001. L. B. acknowledges the Vannevar Bush Faculty Fellowship (VBFF) Grant No. N00014-20-1-2834 from the Department of Defense and the MonArk Quantum Foundry supported by the National Science Foundation Q-AMASE-i program under NSF Award No. DMR-1906383. We thank Prof. Y. Wei at Fudan University for the valuable discussion. The calculation was performed in the high-performance computing center of Jilin University.

*wyc@calypso.cn
†mym@jlu.edu.cn

[1] T. Schäpers, *Semiconductor Spintronics* (De Gruyter, Berlin, 2016).
[2] J. Xia, W. Ge, and K. Chang, *Semiconductor Spintronics* (World Scientific, Singapore, 2011).
[3] H. Wang, P. Gopal, S. Picozzi, S. Curtarolo, M. B. Nardelli, and J. Sławińska, npj Comput. Mater. **6**, 7 (2020).
[4] S. Picozzi, Front. Phys. **2**, 10 (2014).
[5] L. L. Tao and E. Y. Tsymbal, J. Phys. D **54**, 113001 (2021).
[6] Y. A. Bychkov and E. I. Rashba, JETP Lett. **39**, 78 (1984), http://jetpletters.ru/ps/1264/article_19121.shtml.
[7] G. Dresselhaus, Phys. Rev. **100**, 580 (1955).
[8] S. A. Wolf, D. D. Awschalom, R. A. Buhrman, J. M. Daughton, S. von Molnár, M. L. Roukes, A. Y. Chtchelkanova, and D. M. Treger, Science **294**, 1488 (2001).
[9] P. Němec, M. Fiebig, T. Kampfrath, and A. V. Kimel, Nat. Phys. **14**, 229 (2018).
[10] J. Železný, P. Wadley, K. Olejník, A. Hoffmann, and H. Ohno, Nat. Phys. **14**, 220 (2018).
[11] S. Fukami, V. O. Lorenz, and O. Gomonay, J. Appl. Phys. **128**, 070401 (2020).
[12] T. Jungwirth, J. Sinova, A. Manchon, X. Marti, J. Wunderlich, and C. Felser, Nat. Phys. **14**, 200 (2018).
[13] T. Jungwirth, X. Marti, P. Wadley, and J. Wunderlich, Nat. Nanotechnol. **11**, 231 (2016).
[14] L.-D. Yuan, Z. Wang, J.-W. Luo, and A. Zunger, Phys. Rev. Mater. **5**, 014409 (2021).

[15] L.-D. Yuan, Z. Wang, J.-W. Luo, and A. Zunger, Phys. Rev. B **103**, 224410 (2021).
[16] L.-D. Yuan, Z. Wang, J.-W. Luo, E. I. Rashba, and A. Zunger, Phys. Rev. B **102**, 014422 (2020).
[17] K. Yamauchi, P. Barone, and S. Picozzi, Phys. Rev. B **100**, 245115 (2019).
[18] S. A. Egorov, D. B. Litvin, and R. A. Evarestov, J. Phys. Chem. C **125**, 16147 (2021).
[19] S. A. Egorov and R. A. Evarestov, Physica (Amsterdam) **139E**, 115118 (2022).
[20] H. Reichlová *et al.*, Macroscopic time reversal symmetry breaking by staggered spin-momentum interaction, arXiv:2012.15651.
[21] R. Ramazashvili, P. D. Grigoriev, T. Helm, F. Kollmannsberger, M. Kunz, W. Biberacher, E. Kampert, H. Fujiwara, A. Erb, J. Wosnitza, R. Gross, and M. V. Kartsovnik, npj Quantum Mater. **6**, 11 (2021).
[22] H. Wang and X. Qian, npj Comput. Mater. **6**, 199 (2020).
[23] N. Sivadas, S. Okamoto, and D. Xiao, Phys. Rev. Lett. **117**, 267203 (2016).
[24] M. Fiebig, J. Phys. D **38**, R123 (2005).
[25] Note, however, that the coupling $\lambda_{\alpha,\beta}P_\alpha\sigma_\beta$ *does not* exist in materials with time-reversal symmetry, as will be shown below.
[26] Magnetic Point Group Tables, https://www.cryst.ehu.es/cryst/mpoint.html.
[27] W. Hergert and M. Geilhufe, *Group Theory in Solid State Physics and Photonics: Problem Solving with Mathematica* (Wiley-VCH, New York, 2018).
[28] G. F. Koster, J. D. Dimmock, R. G. Wheeler, and H. Statz, *Properties of the Thirty-Two Point Group* (M.I.T. Press, Cambridge, MA, 1963).
[29] S. L. Altmann and P. Herzig, *Point-Group Theory Tables (Second Edition)* (Wien, 2011).
[30] See Supplemental Material at http://link.aps.org/supplemental/10.1103/PhysRevLett.129.187602 which includes symmetry analysis, methods, and some numerical results (e.g., band structures and orbital-projected spin magnetizations regarding $SrFe_2S_2O$ and/or Fe_2TeO_6).
[31] Point Group Tables, https://www.cryst.ehu.es/rep/point.html.
[32] G. Kresse and J. Furthmüller, Phys. Rev. B **54**, 11169 (1996).
[33] G. Kresse and D. Joubert, Phys. Rev. B **59**, 1758 (1999).
[34] P. E. Blöchl, Phys. Rev. B **50**, 17953 (1994).
[35] D. M. Ceperley and B. J. Alder, Phys. Rev. Lett. **45**, 566 (1980).
[36] S. L. Dudarev, G. A. Botton, S. Y. Savrasov, C. J. Humphreys, and A. P. Sutton, Phys. Rev. B **57**, 1505 (1998).
[37] W. R. Inc., Mathematica, Version 12.0, Champaign, IL, 2019.
[38] Materials Project, https://materialsproject.org/.
[39] A. Jain, S. P. Ong, G. Hautier, W. Chen, W. D. Richards, S. Dacek, S. Cholia, D. Gunter, D. Skinner, G. Ceder, and K. A. Persson, APL Mater. **1**, 011002 (2013).
[40] K. Momma and F. Izumi, J. Appl. Crystallogr. **44**, 1272 (2011).
[41] V. Wang, N. Xu, J.-C. Liu, G. Tang, and W.-T. Geng, Comput. Phys. Commun. **267**, 108033 (2021).
[42] VASPKIT, https://vaspkit.com.
[43] J. D. Hunter, Comput. Sci. Eng. **9**, 90 (2007).
[44] SeeK-path, https://www.materialscloud.org/work/tools/seekpath.
[45] Y. Hinuma, G. Pizzi, Y. Kumagai, F. Oba, and I. Tanaka, Comput. Mater. Sci. **128**, 140 (2017).
[46] A. Togo and I. Tanaka, `Spglib`: A software library for crystal symmetry search (2018), arXiv:1808.01590.
[47] H. T. Stokes and D. M. Hatch, J. Appl. Crystallogr. **38**, 237 (2005).
[48] FINDSYM, https://stokes.byu.edu/iso/findsym.php.
[49] M. I. Aroyo, A. Kirov, C. Capillas, J. M. Perez-Mato, and H. Wondratschek, Acta Crystallogr. Sect. A **62**, 115 (2006).
[50] M. I. Aroyo, J. M. Perez-Mato, C. Capillas, E. Kroumova, S. Ivantchev, G. Madariaga, A. Kirov, and H. Wondratschek, Z. Kristallogr. Cryst. Mater. **221**, 15 (2006), https://www.degruyter.com/document/doi/10.1524/zkri.2006.221.1.15/html.
[51] MAGNDATA, http://webbdcrista1.ehu.es/magndata.
[52] S. V. Gallego, J. M. Perez-Mato, L. Elcoro, E. S. Tasci, R. M. Hanson, K. Momma, M. I. Aroyo, and G. Madariaga, J. Appl. Crystallogr. **49**, 1750 (2016).
[53] S. V. Gallego, J. M. Perez-Mato, L. Elcoro, E. S. Tasci, R. M. Hanson, M. I. Aroyo, and G. Madariaga, J. Appl. Crystallogr. **49**, 1941 (2016).
[54] U. Herath, P. Tavadze, X. He, E. Bousquet, S. Singh, F. Munoz, and A. H. Romero, Comput. Phys. Commun. **251**, 107080 (2020).
[55] PYPROCAR, https://romerogroup.github.io/pyprocar/index.html.
[56] A. Manchon, H. C. Koo, J. Nitta, S. M. Frolov, and R. A. Duine, Nat. Mater. **14**, 871 (2015).
[57] MTENSOR, https://www.cryst.ehu.es/cgi-bin/cryst/programs/mtensor.pl.
[58] L. Šmejkal, Y. Mokrousov, B. Yan, and A. H. MacDonald, Nat. Phys. **14**, 242 (2018).
[59] L. Y. Voon, L. C., and M. Willatzen, The $k \cdot p$ Method: Electronic Properties of Semiconductors (Springer, Berlin, 2009).
[60] M. Dresselhaus, G. Dresselhaus, and A. Jario, *Group Theory—Application to the Physics of Condensed Matter* (Springer-Verlag, Berlin Heidelberg, 2008).
[61] Here, the second equality holds because that $\mathcal{E}_\alpha$ polarizes centrosymmetric materials by creating P_α.
[62] H. Guo, M.-T. Fernández-Díaz, A. C. Komarek, S. Huh, P. Adler, and M. Valldor, Eur. J. Inorg. Chem. **2017**, 3829 (2017).
[63] W. Kunnmann, S. L. Placa, L. Corliss, J. Hastings, and E. Banks, J. Phys. Chem. Solids **29**, 1359 (1968).
[64] S. Buksphan, E. Fischer, and R. Hornreich, Solid State Commun. **10**, 657 (1972).
[65] We also numerically found that polarizing Fe_2TeO_6 by $\mathcal{E}_x = 6$ MV/cm causes a tiny Zeeman spin splitting of ∼3 meV at the CBM.
[66] The conventional Zeeman spin splitting created by magnetic field B is given by $|g'|\mu_B B$, where g' is the effective Landé g-factor [1,2]. For free electrons or electrons in non-magnetic semiconductors with large enough band gap, the g' is nearly 2.0 [1,2]. The Zeeman spin splitting of ∼55 meV can be driven by magnetic field of ∼475 Tesla. In II-V wurtzite

semiconductors ZnS and CdSe, the effective $|g'|$ are 2.3 and 0.6, respectively [2]. Generating Zeeman splitting of ~55 meV in ZnS and CdSe semiconductors thus requires a magnetic field of ~413 and ~1583 Tesla, respectively. In III-V semiconductor InSb, the effective $|g'|$ can be as large as 51.3 [2]. In such a case, magnetic field of ~18 Tesla creates Zeeman spin splitting of ~55 meV.

[67] H. Fu and L. Bellaiche, Phys. Rev. Lett. **91**, 057601 (2003).

[68] Given the spinor quantum state $|\psi\rangle$, the expectation value of spin magnetization S_α is defined by $\frac{1}{2}\langle\psi|\sigma_\alpha|\psi\rangle$ ($\alpha = x, y, z$). See, e.g., Ref. [5].

[69] Neglecting the spin-orbit interaction does not qualitatively change our predictions for $SrFe_2S_2O$ and Fe_2TeO_6 (see Fig. S6 of the Supplemental Material).

[70] As for $SrFe_2S_2O$ polarized by $\mathcal{E}_x = \pm 6$ MV/cm, the induced spin splittings are too tiny to detect.

[71] X. Zhang, H.-O. Li, G. Cao, M. Xiao, G.-C. Guo, and G.-P. Guo, Natl. Sci. Rev. **6**, 32 (2019).

[72] V. Baltz, A. Manchon, M. Tsoi, T. Moriyama, T. Ono, and Y. Tserkovnyak, Rev. Mod. Phys. **90**, 015005 (2018).

[73] O. Gomonay, V. Baltz, A. Brataas, and Y. Tserkovnyak, Nat. Phys. **14**, 213 (2018).